Supplementary Material

Volatile Organic Compound Removal by Post Plasma-Catalysis over Porous TiO_2 with Enriched Oxygen Vacancies in a Dielectric Barrier Discharge Reactor

Wenjie Wu[a,b], Saiyu Bu[c], Liang Bai[d], Yenan Song[a,e]*, Yuanting Su[a], Haitao Sun[d], Guangyin Zhen[e], Ke Dong[g], Lunhua Deng[d], Qinghong Yuan[d], Chengbin Jing[a], and Zhuo Sun[a]

[a]Engineering Research Center for Nanophotonics and Advanced Instrument, Ministry of Education, School of Physics and Electronic Science, East China Normal University, Shanghai 200241, China

[b]Collage of Marine Science and Technology, Zhejiang Ocean University, Zhoushan, 316022, China.

[c]School of Mechanical Engineering, Shanghai Jiao Tong University, Shanghai 200241, China

[d]State Key Laboratory of Precision Spectroscopy, School of Physics and Electronic Science, East China Normal University, Shanghai 200241, China.

[e]Joint Institute of Advanced Science and Technology, East China Normal University, Shanghai 200241, China

[f]Shanghai Key Lab for Urban Ecological Processes and Eco-Restoration, School of Ecological and Environmental Sciences, East China Normal University, Shanghai 200241, China

[g] Life Science Major, Kyonggi University, Suwon, South Korea

*Corresponding author：

E-mail: ynsong@phy.ecnu.edu.cn (Yenan Song)

The calculation method for the angles between crystal faces

The theoretical value for the angles (φ) between ($h_1k_1l_1$) and ($h_2k_2l_2$) planes of tetragonal nanocrystal was determined by the following formula:

$$\cos\phi = \frac{\frac{1}{a^2}(h_1h_2+k_1k_2) + \frac{1}{c^2}l_1l_2}{\sqrt{\left[\frac{1}{a^2}\left(h_1^2+k_1^2\right)+\frac{1}{c^2}l_1^2\right]\left[\frac{1}{a^2}\left(h_2^2+k_2^2\right)+\frac{1}{c^2}l_2^2\right]}}$$

DFT calculation method

The theoretical calculations were carried out using the Vienna Ab-initio Simulation Package (VASP). All the calculations were performed based on the projected augmented wave (PAW) method with a generalized gradient approximation (GGA) refined with the Perdew-Burke-Ernzerhof (PBE) functional. The geometry optimization was simulated in the gas phase condition, in which the optimized information was received for an energy less than 1.0×10^{-4} eV/atom, and the force convergence criterion below 0.02 eV/Å. The cutoff energy was set at 400 eV, and the Brillouin zone is sampled by 3×3×1. The vacuum layer in the slab model is more than 15 Å. For the slab information, the (110) surface was chosen as the reaction interface. The atoms of the bottom two layers were fixed, and others could relax.

The adsorption energy of the adsorbate (O_3 and C_7H_8) is defined as follows:

$$E_{ads} = E_{total} - E_{TiO2} - E_{adsorbate}$$

Where E_{ads} is the adsorption energy. E_{total}, E_{TiO2} and $E_{adsorbate}$ is the free energy of the adsorbate modified TiO_2, TiO_2 and adsorbates, respectively.

Characterization

The morphologies of as prepared defective TiO_2 were investigated by scanning electron microscope (SEM, Zeiss Gemini SEM 450) and transmission electron microscopy (TEM, JEOL JEM-2100). The crystal structures were characterized by X-ray diffraction (XRD, PANalytica Empyrean Alpha 1) equipped with Cu Kα radiation (in the

2θ range 10 - 80°). X-ray photoelectron spectroscopy (XPS, Thermo Fisher Scientific Escalab250Xi) was conducted to research the surface chemical states, and all binding energy of the spectrum were calibrated with the C1s photoemission peak at 284.8 eV. The textural characteristics of the catalysts were investigated by using N_2-adsorption and desorption (ASAP2460, Micromeritics) at 77k, the specific surface areas were analysed by the Brunauer-Emmett-Teller (BET) equation, pore volume and average pore diameter were calculated by Barrett-Joyner-Halenda method. Raman spectroscopy measurements were conducted at room temperature using a LabRAM HR 800UV (Horiba) at a wavelength of 532 nm. Fourier-transform infrared spectra were obtained on a Tensor II (Bruker) infrared spectrometer. The fluorescence spectrums were performed on a JY FM-4 fluorescence spectrometer (Horiba) with Xenon lamp as an excitation light source (λ = 362nm). The UV-Vis diffuse reflectance spectra were observed through the U-3900 (Hitachi) with barium sulfate as reference. Electron paramagnetic resonance (EPR) spectrum was carried out on E580-10 (Bruker) at 77k. The hydrogen temperature-programmed reduction (H_2-TPR) and temperature-programmed desorption of O_2 (O_2-TPD) measurements were performed on a AutoChem II2920 (Micromeritics).

Photoelectrochemical Measurements

The Mott-Schottky plots and electrochemical impedance spectroscopy (EIS) were obtained using Autolab PGSTAT 302N electrochemical workstation (Metrohm). 0.1 M Na_2SO_4 aqueous solution was used as electrolytes. The as-prepared TiO_2 samples (5 mg) was dissolved in 500 µL ethanol and 500 µL Nafion stirring ultrasonically for one hour, and then 5.0 µL of the above suspension was coated onto ITO glass (1 cm ×1 cm). This TiO_2 modified ITO glass was used as working electrode, Ag/AgCl electrode and Pt wire were served as reference electrode and counter electrode, respectively. The EIS spectrum was carried out by applying an Ac voltage amplitude of 10 mV, the frequency in the range of 10-10^5 Hz, and bis potential of 0.1 V. The Mott-Schottky were tested at 1000 Hz frequency, and 1mV amplitude.

Qualitative and Quantitative Studies of the ROS

The electron spin resonance (ESR) signals of the reactive oxygen species were qualitatively measured using DMPO and TEMP as trapping agents. Specifically, TiO_2 catalyst powder was dispersed in DMPO/TMPO solution with NTP generated exhaust purging, H_2O was used as a solvent for capturing ·OH and $^1O_2$ species, and methanol was used to capture $\cdot O_2^-$. The NBT method was employed to quantify the concentration of the generated $\cdot O_2^-$.[1, 2] After reacting with $\cdot O_2^-$ species, NBT is transformed into monoformazan and diformazan, and the maximum absorbance peak at 259 nm fades away. The amount of $\cdot O_2^-$ was estimated by measuring the degradation of NBT by UV-visible spectroscopy. The production of ·OH was quantitatively analysed by BA, which readily reacts with ·OH to produce p-hydroxybenzoic acid (*p*-HBA).[3] The concentration of generated *p*-HBA was detected by HPLC with the mobile phase consisting of water/acetonitrile (85/15, v/v) at λ = 270 nm. This value was used to estimate the concentration of ·OH via the equation: [•OH] = [*p*-HBA] × 5.87. In addition, DPBF with an adsorption peak at 410 nm was used as an $^1O_2$ trapping agent to investigate the concentration of $^1O_2$.[4] By testing the reduction in DPBE, the amounts of generated $^1O_2$ were evaluated at a 1:1 molar ratio.

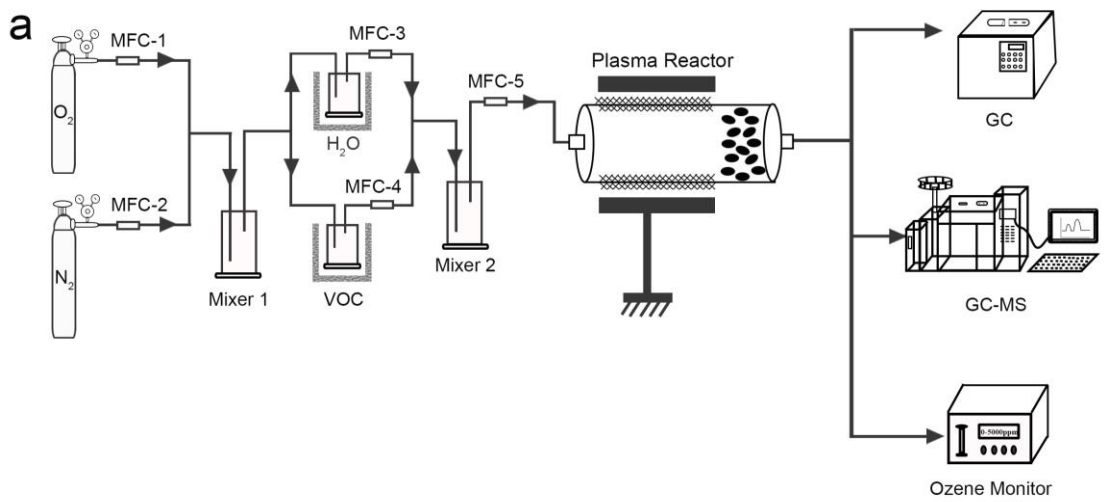

Fig. S1. Schematic diagram of the experimental setup.

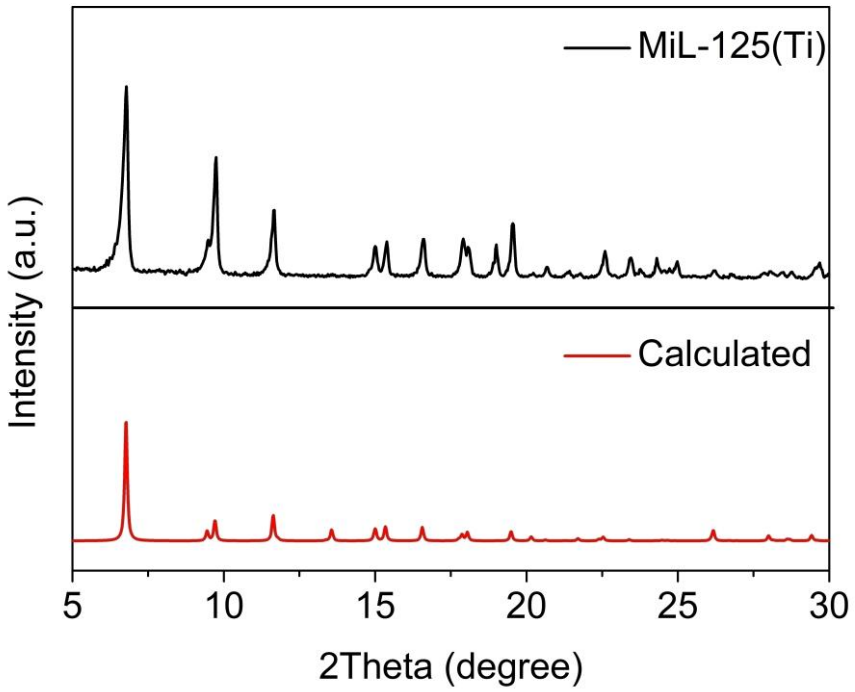

Fig. S2. XRD spectrum of MIL-125(Ti).

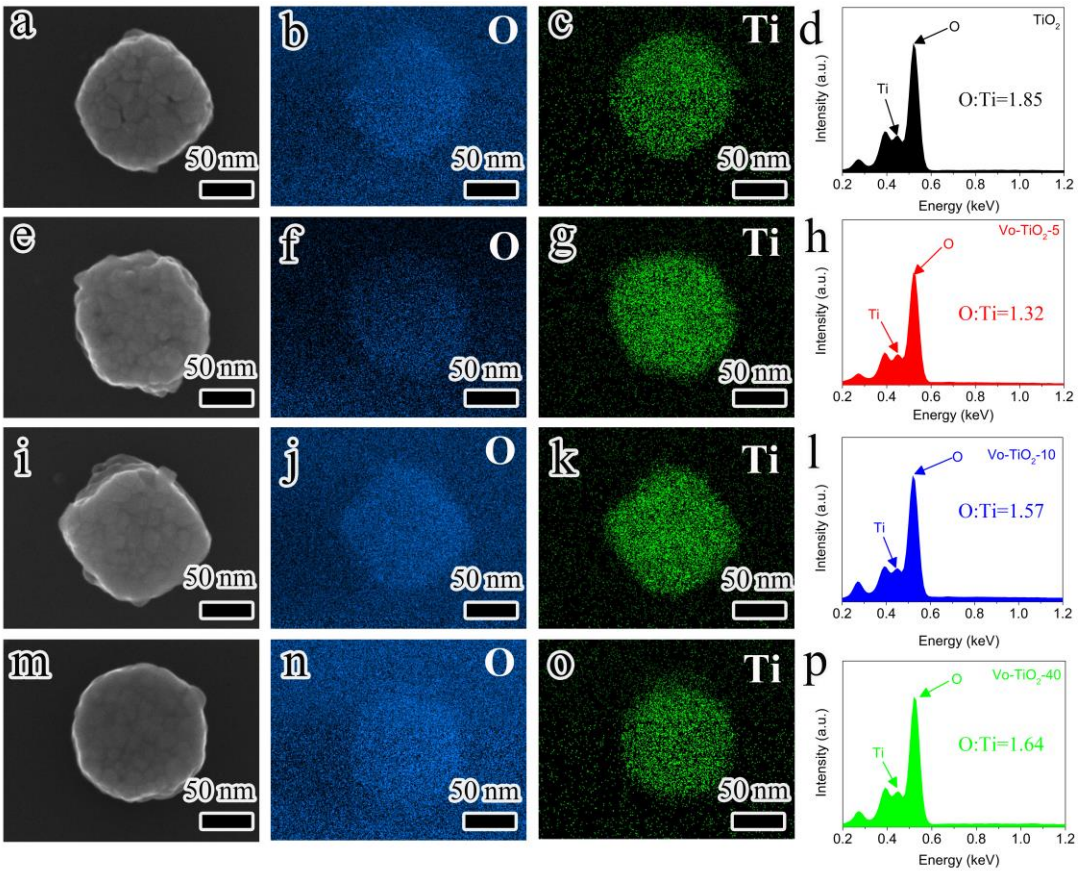

Fig. S3. SEM images and corresponding elements mapping of (a-d) TiO_2, (e-h) Vo-TiO_2-5, (i-l) Vo-TiO_2-10 and (m-p) Vo-TiO_2-40.

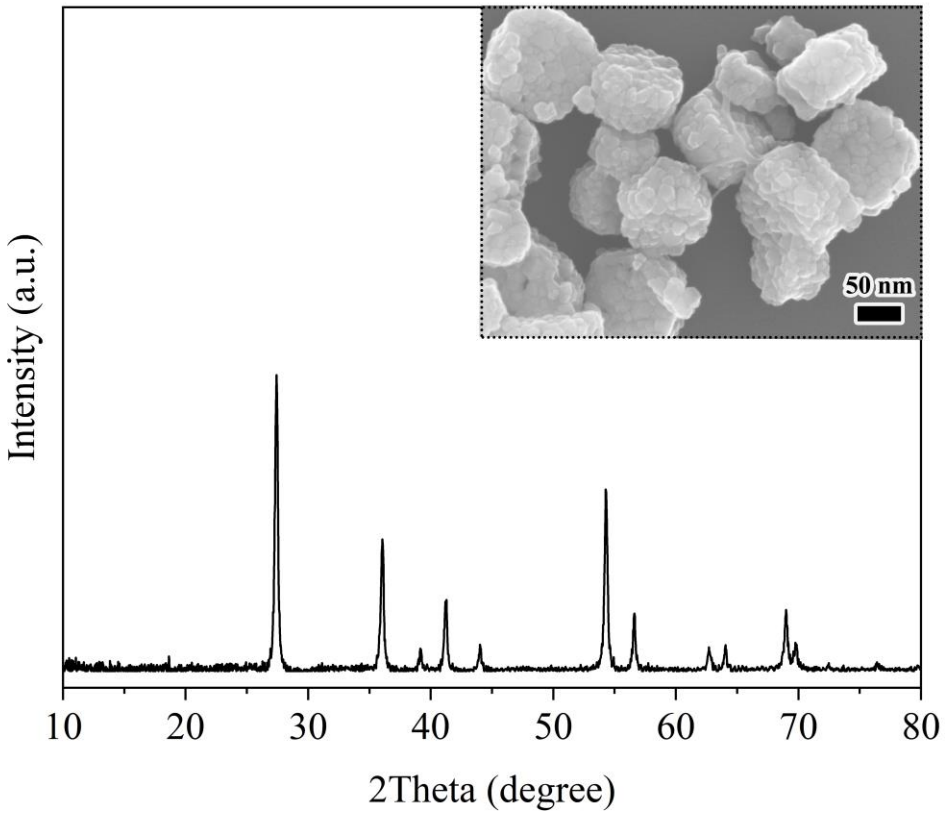

Fig. S4. The XRD spectrum and SEM images of the Vo-TiO_2-5 catalysts after the post-NTP reaction.

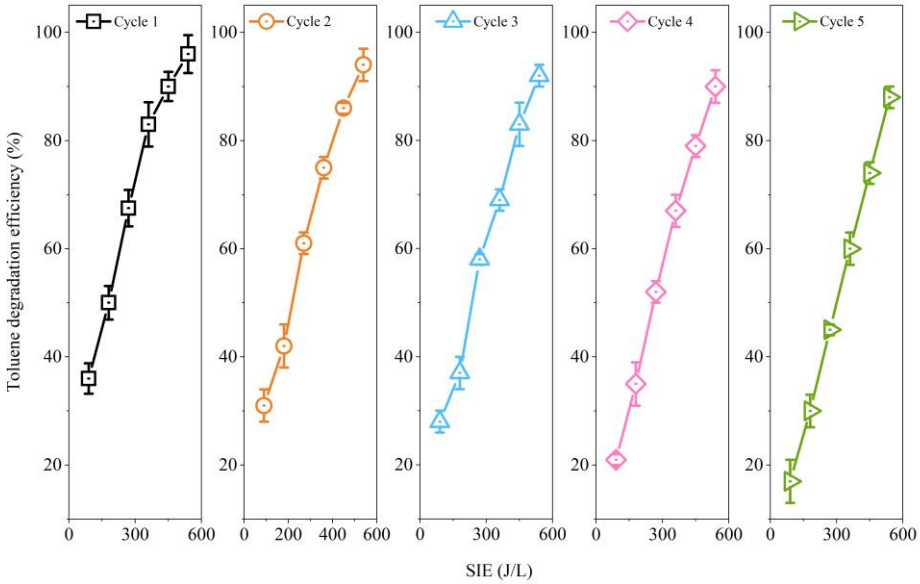

Fig.S5 Stability measurement of the Vo-TiO_2-5 catalyst after 5 cycles.

Table S1. Comparison of degradation of toluene by NTP in the present and previous studies.

Notes: [a] Unit in mL.

Combination mode	Catalysts	Dosages (g)	η_{EY} (g kWh^{-1})	SIE ($J \cdot L^{-1}$)	RH (%)	$\eta_{touluene}$ (%)	Reference
NTP	-	-	2.5	200	85	0	[5]
Post NTP	Ti-Co	0.5	4.28	65	30	72	[6]
Post NTP	MnO_2/AC	1	-	172	0	55	[7]
Packed NTP	γ-Al_2O_3/ZSM-5	37	0.82	88.2	0	100	[8]
Post NTP	Ag-Mn/HZSM-5	1.6	5.4	48	40	63.9	[9]
Solar-enhanced post NTP	MnO_2/GFF	0.0098	8.1	350	0	57.6	[10]
Packed NTP	Mn-Co-Ni	0.2	3.0	444	0	99.7	[11]
Packed NTP	$Ba_{1-x}Ce_xTiO_3$	0.2	-	508.8	0	100	[12]
Packed NTP	CoSMF	-	-	295	0	90	[13]
Post NTP	MnO_2-Co_3O_4	0.1	3.30	423.5	0	92	[14]
Packed NTP	Ag-Mn-O	2	-	35	10	95	[15]

Packed NTP	CeO_2-MnO_x	-	3.39	5760	0	95	[16]
Packed NTP	Au/CeO_2/Al_2O_3	0.15 [a]	0.89	1500	30	99	[17]
Packed NTP	MnOx/SMF	-	5.7	235	0	100	[18]
Post NTP	$MnCoO_x$/γ-Al_2O_3	-	1.86	600	0-70	64	[19]
Post NTP	Vo-TiO_2-5	0.1	5.4	450	40	90	This work

Table S2. N_2 adsorption-desorption measurement results of TiO_2 and Vo-TiO_2-X.

Samples	BET surface area (m^2/g)	Total Pore volume (cm^3/g)
TiO_2	58	0.086
Vo-TiO_2-40	75	0.116
Vo-TiO_2-10	78	0.364
Vo-TiO_2-5	136	0.407

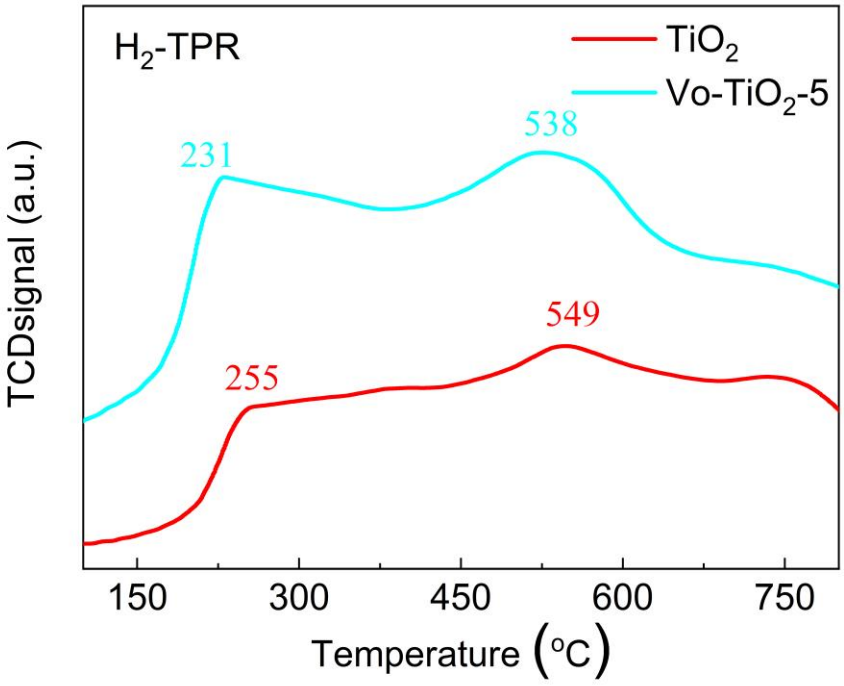

Fig. S6. The H_2-TPR of TiO_2 and Vo-TiO_2-5 sample.

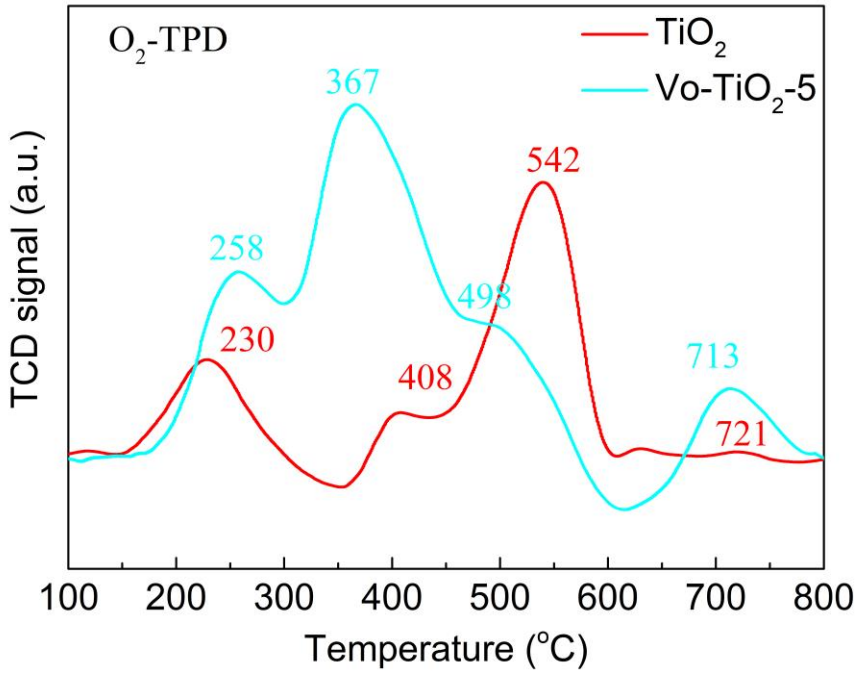

Fig. S7. The O_2-TPD of TiO_2 and Vo-TiO_2-5 sample.

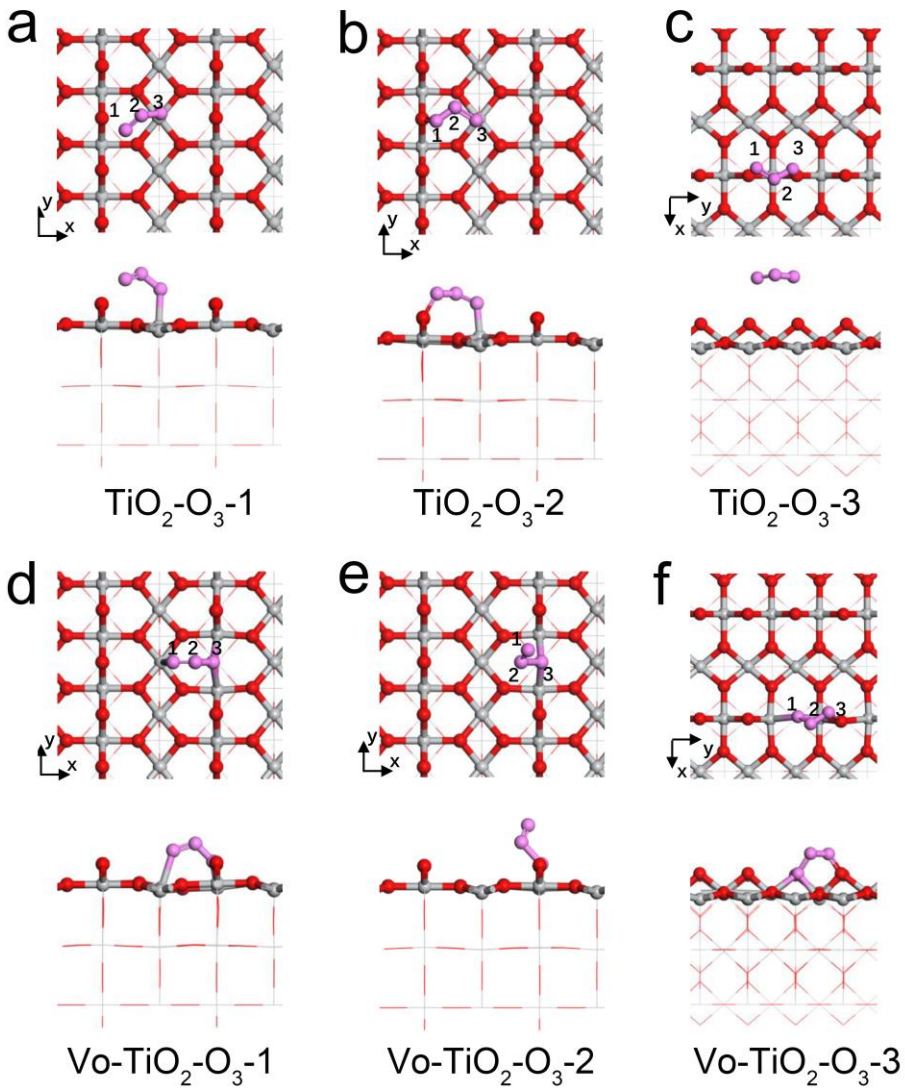

Fig. S8. DFT calculation models for different structures: (a) TiO_2-O_3-1, (b) TiO_2-O_3-2 and (c) TiO_2-O_3-3, (d) Vo-TiO_2-O_3-1, (e) Vo-TiO_2-O_3-2 and (f) Vo-TiO_2-O_3-3.

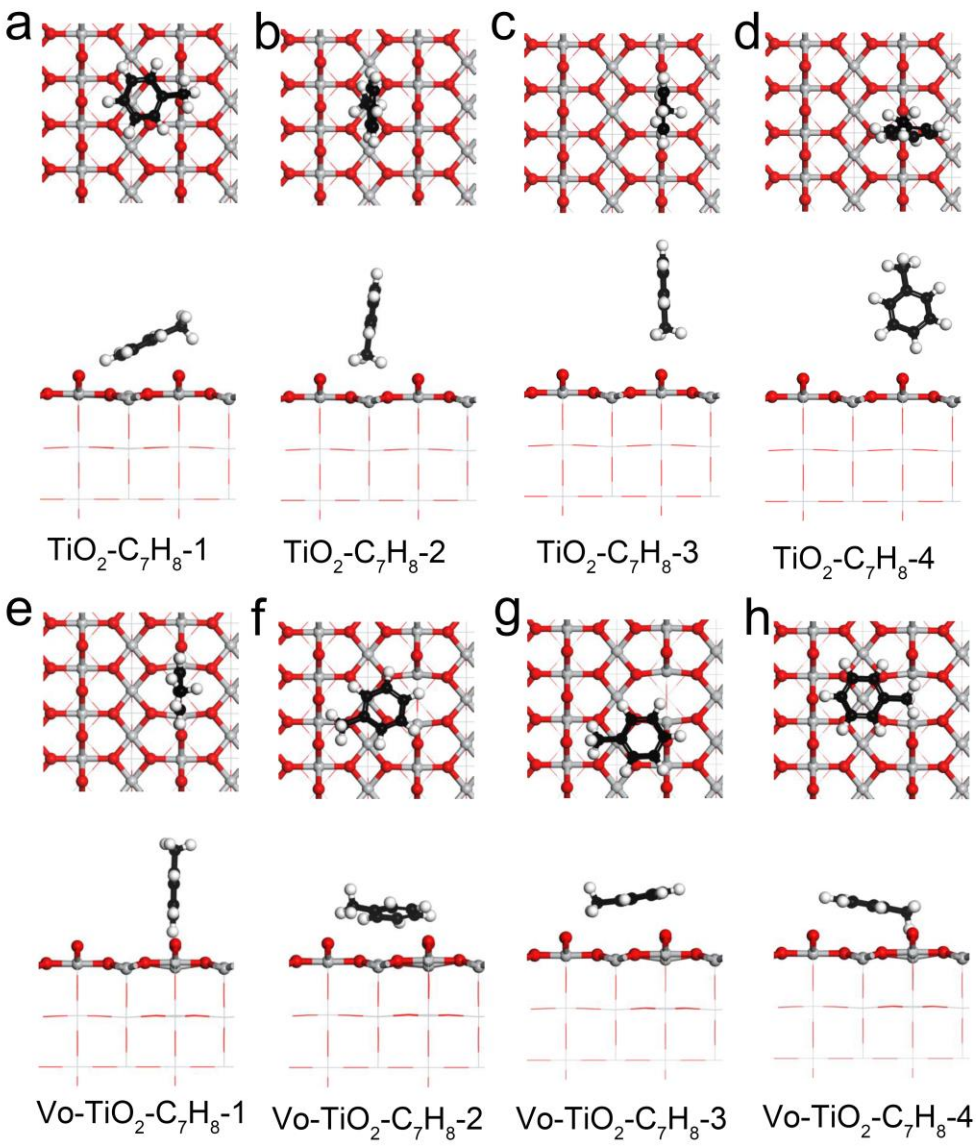

Fig. S9. DFT calculation models for different structures: (a) TiO_2-C_7H_8-1, (b) TiO_2-C_7H_8-2, (c) TiO_2-C_7H_8-3, (d) TiO_2-C_7H_8-4, (e) Vo-TiO_2-C_7H_8-1, (f) Vo-TiO_2-C_7H_8-2, (g) Vo-TiO_2-C_7H_8-3 and (f) Vo-TiO_2-C_7H_8-4.

References

1. Y. Yoko, U. Naoki, R. Akemi, A. Kumi, M. Naoki, G. Yukihiro, M. Toshiki and N. Tetsuo, *J. Am. Chem. Soc*, 2003, **125**, 12803-12809.
2. V. Lakshmi Prasanna and R. Vijayaraghavan, *Langmuir*, 2015, **31**, 9155-9162.
3. L. Ye, J. Liu, Z. Jiang, T. Peng and L. Zan, *Appl. Catal. B-Environ.*, 2013, **142-143**, 1-7.
4. X. Mi, P. Wang, S. Xu, L. Su, H. Zhong, H. Wang, Y. Li and S. Zhan, *Angew. Chem. Int. Edi.*, 2021, **60**, 4588-4593.
5. W. Mista and R. Kacprzyk, *Catal. Today*, 2008, **137**, 345-349.
6. Z. Cheng, C. Li, D. Chen, J. Chen, S. Zhang, J. Ye, J. Yu and D. D. Dionysiou, *Sci Total Environ*, 2019, **692**, 940-951.
7. S. Delagrange, L. Pinard and J. Tatibouet, *Appl. Catal. B-Environ.*, 2006, **68**, 92-98.
8. S. Li, X. Yu, X. Dang, H. Guo, P. Liu and C. Qin, *Chem. Eng. J.*, 2019, **375**, 122027.
9. W. Wang, H. Wang, T. Zhu and X. Fan, *J. Hazard. Mater.*, 2015, **292**, 70-78.
10. Z. Bo, S. Yang, J. Kong, J. Zhu, Y. Wang, H. Yang, X. Li, J. Yan, K. Cen and X. Tu, *ACS Catal.*, 2020, **10**, 4420-4432.
11. X. Feng, C. Chen, C. He, S. Chai, Y. Yu and J. Cheng, *J. Hazard. Mater.*, 2020, **383**, 121143.
12. K. Wu, Y. Sun, J. Liu, J. Xiong, J. Wu, J. Zhang, M. Fu, L. Chen, H. Huang and D. Ye, *J. Hazard. Mater.*, 2021, **405**, 124156.
13. C. Subrahmanyam, A. Renken and L. Kiwi-Minsker, *Chem. Eng. J.*, 2010, **160**, 677-682.
14. T. Chang, Z. Shen, Y. Huang, J. Lu, D. Ren, J. Sun, J. Cao and H. Liu, *Chem. Eng. J.*, 2018, **348**, 15-25.
15. F. Feng, Y. Zheng, X. Shen, Q. Zheng, S. Dai, X. Zhang, Y. Huang, Z. Liu and K. Yan, *Environ. Sci. Technol.*, 2015, **49**, 6831-6837.
16. B. Wang, C. Chi, M. Xu, C. Wang and D. Meng, *Chem. Eng. J.*, 2017, **322**, 679-692.
17. B. Zhu, L.-Y. Zhang, M. Li, Y. Yan, X.-M. Zhang and Y.-M. Zhu, *Chem. Eng. J.*, 2020, **381**, 122599.
18. C. Subrahmanyam, M. Magureanu, A. Renken and L. Kiwi-Minsker, *Appl. Catal. B-Environ.*, 2006, **65**, 150-156.
19. T. Chang, J. Lu, Z. Shen, Y. Huang, D. Lu, X. Wang, J. Cao and R. Morent, *Appl. Catal. B-Environ.*, 2019, **244**, 107-119.